

Article

Optimization Study on Key Technology of Improved Arch Cover Method Construction for Underground Metro Stations Based on Similar Model Test

Wangxing Yang ^{1,2}, Mingkai Xu ^{1,2}, Wenxiang Peng ^{1,2} and Taoying Liu ^{1,2,*}¹ School of Resources and Safety Engineering, Central South University, Changsha 410083, China² China Railway 16th Bureau Group Corporation, Beijing 100018, China

* Correspondence: taoying@csu.edu.cn

Abstract: To enhance comprehension of the improved arch cover construction method for underground metro stations and provide guidance for future construction techniques and programs, the paper examines the indoor improved arch cover method of construction in the underground concealed excavation station of Tianhe Road Station of Guangzhou Metro Line 10, China. It includes a similar model test of the key technology and an analysis of the evolution law of the surrounding rock stress, the law of the ground settlement, and the law of the arch top deformation after the tunnel excavation. The study found that increased over-support can decrease arch settlement, with the maximum settlement occurring near the arch. Ground settlement typically occurs in the same areas as arch settlement, but arch settlement may occur earlier. The excavation of the arch cover has little impact on the overlying soil pressure, and the supporting structure is more effective in controlling soil deformation. The upper part of the arch cap experiences mainly extrusion stress, with the maximum stress occurring near the middle of the arch. The stresses in the arch's base decrease significantly during the excavation of the side drifts but show an increasing trend during the excavation of the lower rock mass. The presence of the central column significantly affects both the settlement of the arch and the ground, as it bears most of the compressive stress of the arch. This stress decreases initially and then increases. The amplitude of deformation is more pronounced when the dismantled central column is closer to the middle of the arch.

Keywords: arch method; similar models; settlement laws; stress evolution; support effects



Citation: Yang, W.; Xu, M.; Peng, W.; Liu, T. Optimization Study on Key Technology of Improved Arch Cover Method Construction for Underground Metro Stations Based on Similar Model Test. *Appl. Sci.* **2024**, *14*, 3982. <https://doi.org/10.3390/app14103982>

Academic Editor: Tiago Miranda

Received: 29 March 2024

Revised: 2 May 2024

Accepted: 3 May 2024

Published: 8 May 2024



Copyright: © 2024 by the authors. Licensee MDPI, Basel, Switzerland. This article is an open access article distributed under the terms and conditions of the Creative Commons Attribution (CC BY) license (<https://creativecommons.org/licenses/by/4.0/>).

1. Introduction

The urban agglomerations in different countries are showing a trend of concentration due to the continuous development of the economy. This has led to the gradual acceleration of the urbanization process and the expansion of city scales, increasing the population of large and medium-sized cities [1]. However, this has also led to road congestion, frequent traffic accidents, and commuting inefficiencies. The negative impacts of urbanization, including those caused by the expansion of surface roads, are deepening. The cost of maintaining these roads is high, making it necessary to find alternative solutions [2–4]. The rational use of urban underground space and the construction of subways have become effective means of alleviating this social contradiction. Metro construction is a complex process, particularly when it comes to building metro stations in busy urban areas. The geological environment must be taken into account, as well as the impact on surrounding buildings, pipelines, and traffic routes. The arch cover method is a concealed excavation construction technique that utilizes the self-stability of surrounding rock and employs appropriate reinforcement. This method is highly efficient, has a small impact range, and is very flexible. However, this method is still affected by the rock conditions, the grade of the surrounding rock, and other factors in actual engineering use. Therefore, carrying out an optimization study of the key technology for the construction of the arch cover method will

have significant engineering significance for its applicability. This study can provide better guidance for subsequent underground construction. Selecting the appropriate method according to local conditions can reduce construction costs and bring about higher economic and social benefits.

Figure 1 shows the schematic section of the arch cover method. In the construction of the arch cover method, the construction of overrun support is carried out first. The center drift (A) was then excavated using the center diaphragm method and promptly primed. Subsequently, the anchor rod inserted on the right side of the center drift (A) shall be removed, followed by the excavation of the center drift (B). It is imperative that the distance between the faces of center drift (A) and center drift (B) is maintained at no less than 5 m. Additionally, within the center drifts, construction activities include the installation of steel pipe columns, segmental arches for the roof, and longitudinal beams. Upon completion of these construction tasks, the partition walls shall be dismantled. However, the length of each dismantling operation should not exceed the span length of the main structure. Furthermore, the excavation work for the side drifts should commence only after the completion of secondary lining construction in the arch sections. Excavation of the side drifts and the construction of the side partition walls are to be carried out concurrently. It is imperative that the distance between the faces of side drift (A) and side drift (B) is maintained at no less than 8 m to mitigate the risk of group cavity effects. Subsequently, the side partition walls and the bottom slab are to be dismantled, followed by the excavation of the lower second layer from the transverse passage location, and the construction of the sidewalls.

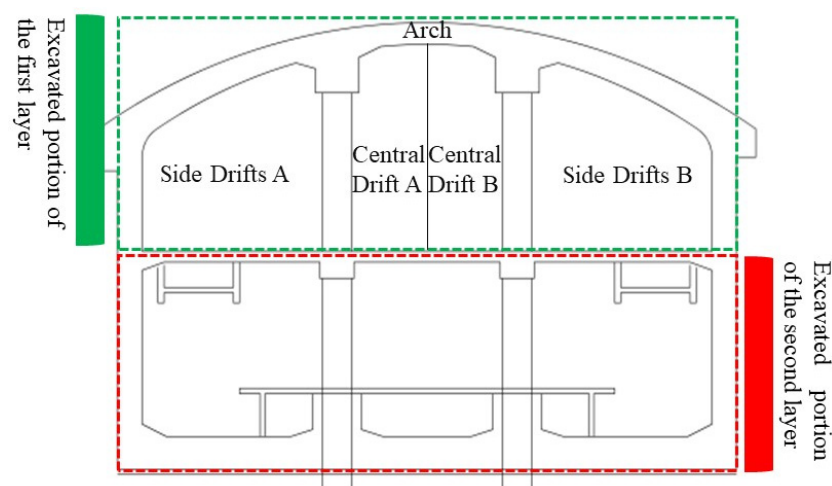


Figure 1. Schematic diagram of underground station excavation by arch cover method.

In the study of the underground shallow buried station dark method, Liu [5] conducted a study on 30 underground stations in the Beijing area which were constructed by the Pile Boring Act (PBA) and concluded that the ground settlement in the first and third phases of the construction by the PBA accounted for 90 percent of the total surface settlement, and the second and fourth phases accounted for 10 percent of the surface settlement. Fang [6] summarized the ground settlement data of the shallow excavation method used in nine underground stations in Beijing and systematically illustrated the effect of shallow excavation on ground settlement. Qingdao area has better surrounding rock conditions, because of which the research and innovation for Qingdao area concealed excavation is still in progress. Liu [7] used Flac3D to study an underground road in Shenzhen and introduced a construction method to control the deformation of the underground bulge. Shang [8] summarized the nature of the upper soft and lower hard rock formations in an underground in Dalian and used numerical simulation to analyze the support effect of six support schemes on the deformation of the surrounding rock. Wang [9] used numerical simulation to compare the applicability of the initial arch cover method and the double sidewall

guide pit method in an underground in Guiyang and concluded that the applicability of the initial arch cover method is better. Lai [10] used numerical simulation and on-site monitoring methods to introduce the two schemes of force conversion between shaft and cross-passage construction and concluded that the parallel structure of the shaft-cross passage is more conducive to controlling shaft deformation. Some scholars use 3D printing technology to simulate the ground load during tunnel excavation, to study the complex ground deformation [11]. Seo [12] presented a comparison of the support effect of the pre-support nailing method with the traditional support method, and the pre-support nailing is more effective in controlling the ground settlement in the shallow underground excavation method. Kishida [13] investigated the effectiveness of the improved geological method for weak strata using numerical simulation and experimental analysis based on the fact that the improved geological method has not yet formed a standardized design basis in the Japanese region. Cao [14] analyzed the field monitoring data by taking an underground station in Beijing as an example, and the study showed that the surface settlement was mainly caused by shield tunneling, side alley excavation, and double-arch excavation. Shen [15] analyzed the on-site monitoring data of the PBA method, discussed the deformation trend of the tunnel at different construction stages, and gave the ground settlement curves. Liu [16] based on the PBA method of an underground station in Beijing, put forward the settlement and other parameter control standards of the project through numerical simulation combined with the on-site monitoring method. Xu [17] presented the monitoring data of the initial PBA method in China, demonstrating that the maximum surface settlements observed across different monitoring sections were not uniform. The author concluded that surface settlement was primarily attributable to the construction of the shield tunnel, the side guideway, and the middle guideway. Tian [18] carried out a four-stage study on the deformation characteristics of the tunnel and the slopes by using on-site investigations, geological boreholes, and measurements, and concluded that the tunnel arch may be forced to squeeze without sliding when it is in the potential landslide zone.

In an indoor similar model test study, Liu [19] conducted a one-factor sensitivity analysis using a model box test and numerical simulation and concluded that increasing the pile diameter of the side piles is better able to control the displacement of the side piles than decreasing the pile spacing in the PBA method. Wang [20] relies on an underground station in Qingdao to establish a large-size model box, gives the design scheme of the model box, and analyses the soil deformation law caused by the tunnel excavation process. Liu [21] used similar model tests to simulate the construction process of a metro station by the hole pile method under the conditions of two surrounding rock levels and four construction schemes, to analyze the mechanical behavior of excavation and to compare with the numerical simulation results. Lei [22] investigated the effect of the bias angle on the lateral pressure of the surrounding rock under asymmetric horizontal loading using three bias model tests with different inclination angles, and the more the bias angle increases, the pressure of the surrounding rock on the shallow buried side gradually decreases. Xiao [23] used a large-size model box to study the deformation force characteristics of tunnels under bias pressure in soil rock junction strata and concluded that the addition of retaining walls to rock slopes can effectively reduce the surrounding rock stresses inside the slopes. Li [24] studied the construction scheme of expanding excavation to build an underground station with three consecutive arches on the basis of an existing shield tunnel through similar model tests. The study demonstrated the support effect of double rows of small catheter overrun grouting reinforcement on tunnel expansion.

In summary, it is evident that indoor model testing has become the primary research method for the construction technology of underground metro station concealed excavation method. Therefore, this paper analyzes the optimization of key technology for the improved large-span arch construction, using the underground station project of Tianhe Road Station of Guangzhou Metro Line 10 in China as a case study. The model box test is employed to investigate the evolution of peripheral rock stress law, ground settlement law, and arch deformation law after tunnel excavation. The results verify the applicability and

reasonableness of the improved arch construction and optimize the construction scheme of the arch construction method. The structure of the research can offer valuable guidance for developing the subsequent construction technology and scheme for this method.

2. Indoor Test

2.1. Similar Materials Test

The similarity test is a widely used research method that is based on the similarity theorem. This theorem uses a certain similarity ratio to the original rock produced in the field to conduct a series of indoor tests. The data recorded by the test are then used to deduce the field situation and solve any engineering problems that may arise during the actual project. To accurately reflect the deformation characteristics and effects of the surrounding rock and support during tunnel excavation, it is important to establish a clear relationship between the simulation prototype and the test model.

The First Similarity Theorem explains the nature of similar phenomena, which refers to a group of phenomena sharing identical equations and criteria. When determining similar phenomena, two conditions must be satisfied: firstly, the ratios of corresponding physical quantities in similar phenomena should remain constant, encompassing geometric, kinematic, dynamic, and other factors; secondly, similar phenomena can be described by the same fundamental equations, meaning both the prototype and the model must adhere to the basic equations of elasticity theory: equilibrium equations, geometric equations, and boundary conditions. The Second Similarity Theorem leverages the relationships among physical quantities to express the intrinsic relationships of physical processes or phenomena. If a physical process or phenomenon cannot be described by equations, but a certain physical quantity has a decisive impact on the research subject, similarity criteria can be determined through dimensional analysis. The Third Similarity Theorem, also known as the Existence of Similarity Theorem, posits that for phenomena of the same kind, if they satisfy the condition that the numerical values of their similarity criteria for single-valued quantities are equal, then these phenomena are considered to be mutually similar.

The physical parameters of the specimens involved in this test contain compressive strength (σ), material strain (ε), angle of internal friction (φ), Poisson's ratio (μ), unit weight (γ), model test displacement (χ), elasticity modulus (E), model dimensions (L) and cohesive (c). Based on the similarity triple theorem [25,26], it can be seen that the relationship equation between different variables is as shown in Equation (1).

$$f(\sigma, \varepsilon, \varphi, \mu, \gamma, \chi, E, L, c) = 0 \tag{1}$$

Calculations are available based on the method of quantitative analysis:

$$F\left(\sigma, \varepsilon, \varphi, \frac{\gamma L}{\sigma}, \frac{\chi}{L}, \frac{E}{\sigma}, \frac{\chi}{\sigma}, \frac{c}{\sigma}\right) = 0 \tag{2}$$

The derivation of the similarity ratio relationship for each physical quantity yields:

$$\begin{cases} C_\varepsilon = 1 \\ C_\varphi = 1 \\ C_\gamma C_L = C_\sigma \\ C_\chi = C_L \\ C_E = C_\sigma \\ C_c = C_\sigma \end{cases} \tag{3}$$

In Formula (3), C_ε , C_φ , C_γ , C_L , C_χ , C_E and C_c are similar ratios of σ , ε , φ , μ , γ , χ , E , L and c . Meanwhile, this paper focuses on the Tianhe Road station, which has an overburden depth of approximately 19 m. The main body of the station is 16 m deep, with a cross-section width of 27.7 m on both sides. The dimensions of the model box used for the test were 1.8 m in height, 1.8 m in length, and 1.0 m in width. The mechanical parameters of

the specimen included compressive strength, weight, and modulus of elasticity. Using the similarity triple theorem, the geometric similarity ratio of the test was calculated to be 35. The formula is shown in Equation (4).

$$C_L = L_H/L_M = 1/35 \quad (4)$$

where C_L is the geometric similarity ratio. L_H is the model geometry. L_M is the prototype geometry. The rock material test specification requires a cylindrical specimen with a diameter of 50 mm and a height of 100 mm. To account for potential contingencies, three samples were produced for each group. The nature of the surrounding rock in which the station is located determines the stability and deformation conditions of the station, and the rock layers in which the metro station is located contain a variety of rock samples such as slightly weathered sandstone, moderately weathered sandstone, bedrock, and so on (Table 1). In order to reduce the station simulation task, all the lower enclosing rocks can be made of slightly weathered muddy siltstone (IV grade) as a safety redundancy.

Table 1. Petrophysical parameters of different strata of the tunnel.

Stratigraphic Rock Name	Natural Density/g/cm ³	Deformation Modulus/MPa	Compressive Strength/MPa	Basic Rock Quality Grade
Strongly weathered conglomerate	2.10	100.0	4.5	V
Strongly weathered siltstone	2.05	95.0	3.62	V
Medium-weathering conglomerate	2.61	3000.0	34.31	IV
Slightly weathered conglomerate	2.66	8000.0	41.83	IV
Slightly weathered siltstone	2.62	7000.0	22.12	IV
Slightly weathered silty sandstone	2.60	5000.0	22.12	IV

The paper selects barium sand, P.O42.5 cement, river sand, and water as raw materials for creating similar materials. Cement serves as a binder and river sand acts as an aggregate. Barium sand functions as a weight enhancer. The material should be weighed in accordance with the appropriate proportion, mixed thoroughly using a mixer, and then water should be added quickly. The mixture should be poured evenly into the mold, and the filling of the specimen should be completed. After demolding, the specimen should be left to solidify at room temperature of 26 °C for 3 days. The weight was measured using an electronic balance. The compressive strength and modulus of elasticity were measured using a uniaxial compression device. The detailed orthogonal scheme and test results are shown in Table 2. Table 3 presents the results of the comparison between similar materials and the original rock test. As shown in the table, the compressive strengths of the specimens from groups 7 and 8 meet the requirements. Therefore, proportion 8 was chosen as the analog rock sample after considering similar materials (cement: water: river sand: barium sand = 2.5:5:30:20).

Table 2. Orthogonal design experimental program.

Test Group	Cement	Water	River Sand	Barium Sand	Unit Weight (kN/m ⁻³)	Compressive Strength/MPa	Elastic Modulus/GPa
1	1.5	4	30	20	23.1	0.3	0.04
2	1.5	4	40	10	21	0.09	0.02
3	1.5	5	30	20	22.9	0.31	0.08
4	2	4	30	20	23.0	0.55	0.05
5	2	4	40	10	20.8	0.22	0.06
6	2	5	30	20	22.8	0.5	0.06
7	2.5	4	30	20	22.9	0.65	0.09
8	2.5	5	30	20	22.8	0.68	0.12
9	2.5	5	40	10	20.6	0.45	0.08

Table 3. Test parameters of similar material specimens.

Specimen	Unit Weight (kN/m ³)	Elastic Modulus/MPa	Compressive Strength/MPa
Engineering rock	26	5000	22.12
Similar material	22.9	120	0.68
Similarity ratio	1.13	41.67	32.53

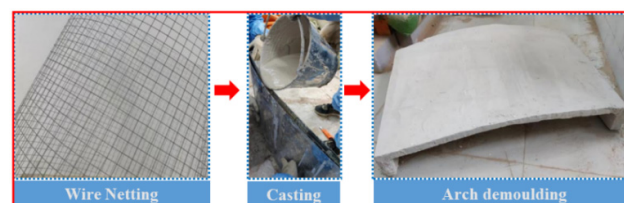
2.2. Similar Model Test

In the similar model indoor tests, the paper carried out similar model tests for arch caps, concrete shotcrete, hand-dug piles, central partition walls, and side partition walls. Among them, the concrete simulation material is generally chosen to be construction gypsum, which has the characteristics of better adhesion and rapid solidification. Due to the short solidification time of gypsum, the parameters can be measured 8 h after fabrication and the test results are shown in Table 4.

Table 4. Similarity ratio of physical parameters of similar materials for concrete.

Concrete	Elastic Modulus/GPa	Compressive Strength/MPa
Engineering concrete	30	30
Similar material	0.83	1.1
Similarity ratio	38.0	27.27

The supporting pile body molds were simulated using bored piles made of 5 cm diameter, 2 mm thick circular hollow steel pipe piles. These piles were pre-built into the model box along with the filled-in rock material before the excavation of the arch cap. However, the top of the pile is not connected to the arch cover part, which means that the arch cover force cannot be transferred to the supporting pile at the beginning. The arch cover is produced using prefabricated gypsum boards to simulate the over-support and initial support. Iron is used as a gypsum mold with a reinforcing mesh made of wire mesh with an aperture of 1.5 cm and a diameter of 0.08 mm for casting. The experimental ratio of gypsum to water is 1:2. After pouring, the arch cover needs to be left for more than 8 h to allow for complete solidification. Please refer to Figure 2 for the test material and model.

**Figure 2.** Arch cover casting process.

The height of the test model box was 1.8 m. The buried depth of the overburden in the prototype station was 19 m, and the longitudinal depth was 16 m. According to similar scale calculations, the buried depth of the overburden in the model box was 54.3 cm, and the longitudinal depth was 45.7 cm. The tunnel's location was marked on the Plexiglas using lines and points. The Plexiglas were then cut with an angle grinder to achieve a 1:35 similarity ratio of the station section with the arch cover. In the process of model backfilling, the lower soil mass is initially filled. Following the specified proportions, a predetermined mass of soil sample is weighed each time and filled from the bottom of the model box to the bottom position of the retaining pile structure. During the filling process, the sample is compacted every 100 mm, with a compacted area of approximately 50 mm. Subsequently, the installation of support piles is carried out. Gypsum material is injected into the interior of the support piles to fabricate precast steel pipe piles. A cement base is constructed at the bottom of the piles to simulate the in situ grouting reinforcement of the

strata at the pile base. Moreover, to prevent the piles from being subjected to load before the secondary lining is applied, certain voids are left at the top of the piles and the crown position. Following this, the installation of the arch cover and the addition of monitoring devices are carried out. To prevent damage to the strain gauges due to the movement of the arch cover, the experiment involves affixing the arch cover after it is placed into the model box. When burying the soil pressure box, the corresponding positions are determined and fixed with tape at the arch crown to prevent displacement during the filling of the upper soil. During the installation of displacement meters, the meters are first placed into PVC pipes and then filled with sand to prevent damage. Moreover, the PVC pipes are fixed to the inner side of the model above the arch crown to prevent sliding and resulting in errors in displacement meter readings. Additionally, to ensure the fixed position remains stable, the lower end of the displacement meter should also be in contact with the arch crown. Finally, the upper overlying soil is continuously filled until reaching the design height. Ground settlement monitoring devices are then secured above, completing the model construction process.

Data monitoring is an important factor affecting the accuracy of indoor modeling tests. The paper involves the collection of four data during the test: earth pressure, displacement, strain, and stress. The collection equipment to be used includes displacement sensors, strain gauges, earth pressure boxes, and percent monitoring. The earth pressure box adopts strain type miniature of the earth pressure box, the product can measure all kinds of contact surface pressure and earth pressure can monitor the trend of earth pressure change in the construction process, small volume, and high sensitivity. The earth pressure calculation formula and earth pressure box technical indicators as shown in formula (5) and Table 5. Where P is the value of soil pressure. $\mu\epsilon$ is the value of micro-strain and K is the sensitivity factor.

$$P = \mu\epsilon \times K \quad (5)$$

Table 5. Main technical specifications of the earth pressure box.

Earth Pressure Box	Impedance/ Ω	Electrical Insulation Resistance/ $M\Omega$
Standard	400	≥ 200

The strain monitoring chooses long strip strain gauges that can measure the deformation parameters of the supporting structure itself, using the change in resistance of the strain gauges under pressure or tension to calculate the bending deformation of the structure body. The displacement meter uses the JMDL-2015A universal displacement meter from Gold Code Hi-Tech, with a range of 50 mm and an accuracy of 0.01 mm. The precision range accuracy of the percentage monitoring is 0.01 mm, and magnetic support is set behind the table and fixed to the angle model box. In addition, the test data acquisition equipment altogether used Donghua's DH3817F dynamic and static strain test and analysis system to collect soil pressure and strain and the supporting JMZX-7000 comprehensive tester to collect displacement meter data. The monitoring equipment and analysis device are shown in Figure 3.

For the indoor tunnel excavation model, the excavation process is simulated realistically by strictly following the on-site construction process. The detailed excavation method is shown in Figure 4, with two excavation cycles carried out in each central drift. During construction excavation, the displacement meter's initial and final values are measured and recorded before and after each excavation condition, respectively. A waiting period of at least 1 h is necessary before proceeding to the next excavation condition. The displacement meter and other data were recorded multiple times during the period until stable data were obtained. These were then combined with real-time stress-strain sensor readings to assess stability. The displacement before excavation, i.e., the stable displacement of the previous working condition, was determined by taking the last measured data before the

excavation of the next working condition. It was confirmed that there were no errors before proceeding to the next construction step.

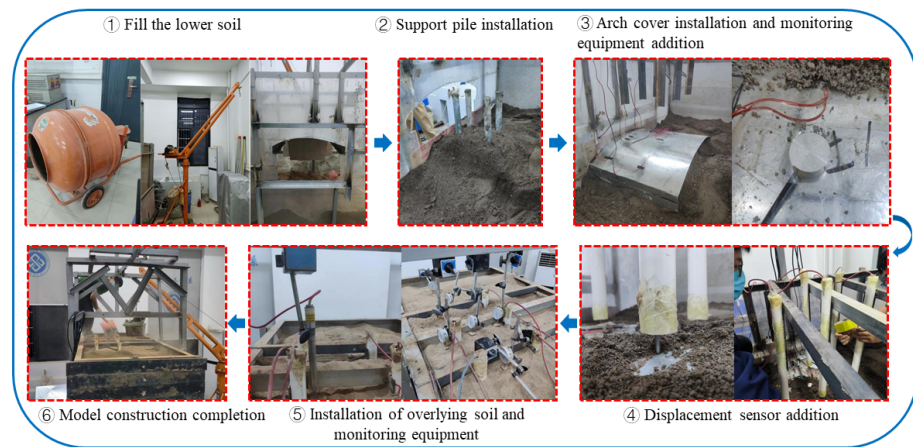


Figure 3. Sequence of similar model construction.

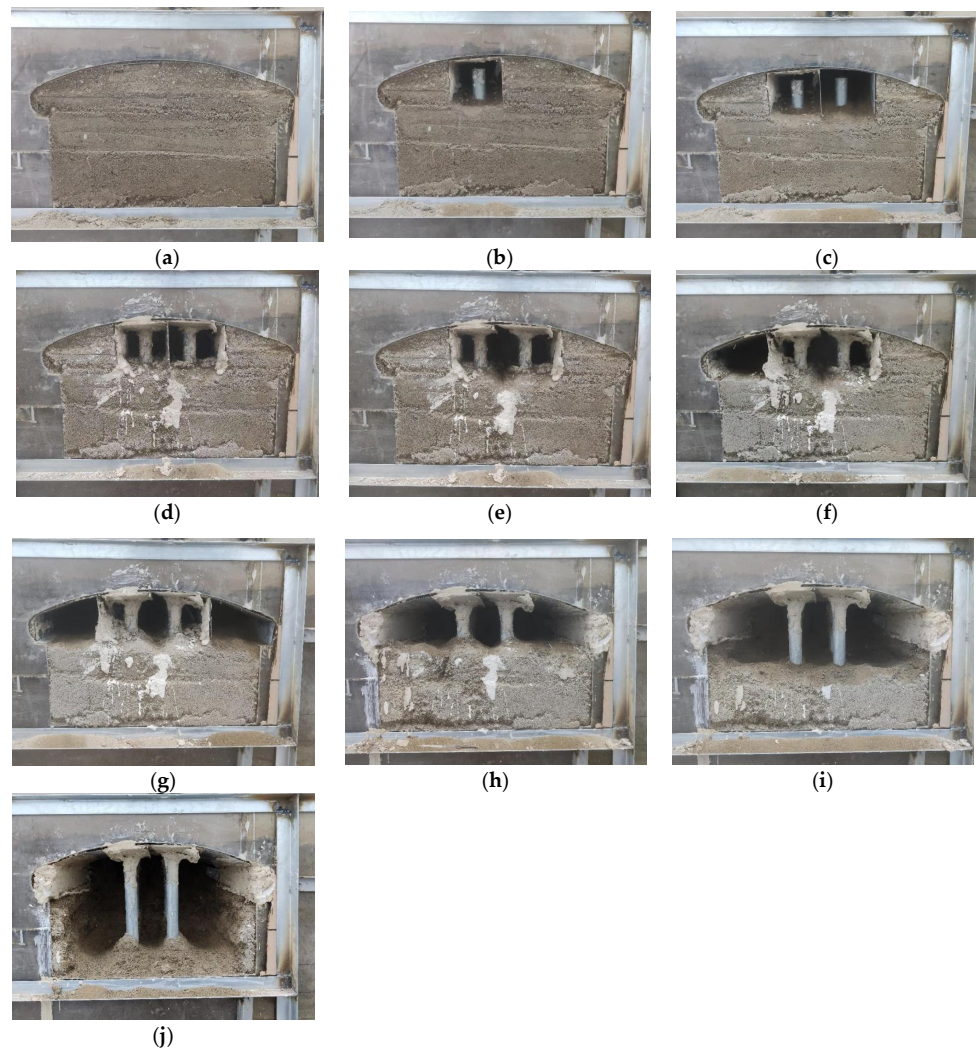


Figure 4. Detailed excavation scheme for tunnel similarity model. (a): Model Excavation Preparation, (b): Excavation of center drift A. (c): Excavation of center drift B. (d): Pile Top Support Construction. (e): Initial support for removal of partition wall. (f): Excavation of side drift A. (g): Excavation of side drift B. (h): Removal of primary support from side partition wall. (i): Excavate downwards once. (j): Excavate downwards twice.

3. Results and Analysis

3.1. The Pattern of Change in the Settlement Pattern of the Arch

Monitoring points were set up 20 cm and 45 cm away from the initial excavation face, respectively, which were used to monitor the arch and both sides of the arch haunch. Among them, the arch haunch is located above the side drifts. The monitoring results and monitoring methods are shown in Figure 5. Table 6 shows the classification results of similar models for critical excavation conditions. The analysis of Figure 5 and Table 6 shows that excavation conditions from 1 to 9 involve the excavation of the central drift, with each drift being excavated in two cycles. At this point, arch displacement begins to occur, with a concentration on the faster rate of change in the arch position. In the 12th excavation condition, the temporary support for the diaphragm wall was removed, resulting in rapid settlement of the arch. Following the removal of the diaphragm wall, excavation of the side drift commenced. At this point, the arch haunch began to settle, and the rate of settlement of the arch top stabilized. In the 18th excavation condition, the initial support of the side partition wall was removed, resulting in a small settlement of the arch. After further excavation of the soil below, there was once again an acceleration of arch settlement. Simultaneously, the maximum settlement of the gypsum arch is 0.3 mm. This indicates that the superior over-supporting method significantly reduces the settlement displacement of the arch during construction. The settlement values of the monitoring section at 20 cm were lower than those at 45 cm.

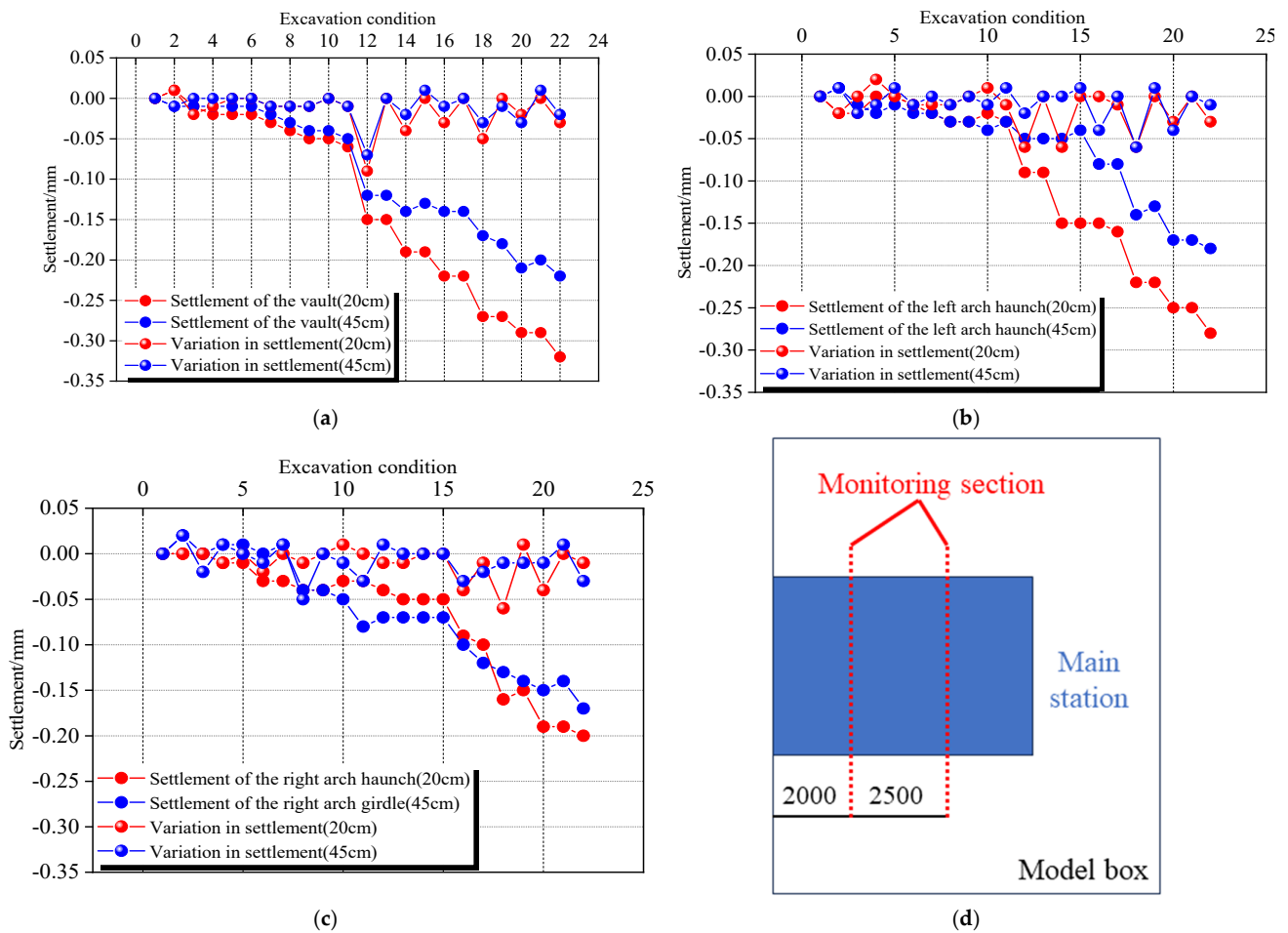


Figure 5. Tunnel monitoring arrangement and monitoring results. (a): Settlement in the middle of the arch. (b): Settlement of the left arch haunch. (c): Settlement of the right arch haunch. (d): Arrangement method of cross-section monitoring points.

Table 6. Classification of critical excavation conditions.

Excavation Condition Number	Classification of Excavation Conditions
1–9	Excavation of the central drift
10–12	Removal of temporary support for partition wall
13–18	Excavation of the side drift
19–20	Removal of initial support for side partition wall
21–22	Excavation of the soil below

Combining the displacement results, it is evident that the removal of the temporary diaphragm wall support has a more significant impact on the settlement in the middle of the arch cap. The removal of the diaphragm wall caused an incremental settlement of 17.39% of the total settlement at the top of the diaphragm wall, but the removal of the temporary side diaphragm wall had a more significant effect on the settlement of the arch haunch. The removal of the temporary diaphragm wall had a greater impact on the overall settlement of the arch cover. Therefore, on-site construction should strictly control the distance of each removal of the diaphragm wall and timely construct the backcasting section above the diaphragm wall to improve the integrity of the support structure. This can reduce the risk of settlement caused by the removal of the side diaphragm wall initial support. Furthermore, upon completion of the upper arch cover construction, the arch's foot will be positioned above the lower surrounding rock. Excavation work will then disturb the support structure of the arch feet, resulting in the settlement of the upper arch. Therefore, during the construction process, it is crucial to reinforce the surrounding rock where the arch's foot is located before excavating the main body below.

3.2. Patterns of Change in Ground Settlement

Figure 6 displays the layout and results of the ground settlement monitoring. The arch and ground settlement exhibit a similar trend, with an increase in the arch settlement resulting in a corresponding increase in the ground. The rate of settlement growth is faster during the removal of temporary supports, excavation of side drift, and excavation of the lower body. The largest incremental ground central settlement, accounting for 16.7% of the total settlement, resulted from the removal of the partition wall. During the model test, the ground settlement was greater than the arch, with the maximum value at Point 6. Specifically, the peak settlement at the central near the outer excavation face is 1.07 mm, which converts to 37.45 mm when using the similarity ratio. The settlement trend of the general area is consistent with the arch. The tests showed that construction excavation had a quicker effect on arch settlement, but a longer effect on ground. Arch settlement can quickly reach a steady state under certain conditions, while ground settlement takes longer to stabilize.

It is prudent to exercise caution when excavating lower rock layers above a sandy stratum, as this may disturb the upper soil, resulting in vibration liquefaction and uneven ground settlement. In extreme cases, the ground settlement value may exceed the amount of settlement of the arch. Therefore, it is essential to utilize small machinery for digging and to monitor any uneven ground settlement throughout the construction process. In the event of construction on significant ground, it is imperative to reinforce ground settlement monitoring and implement strategies to regulate substantial deformation settlement.

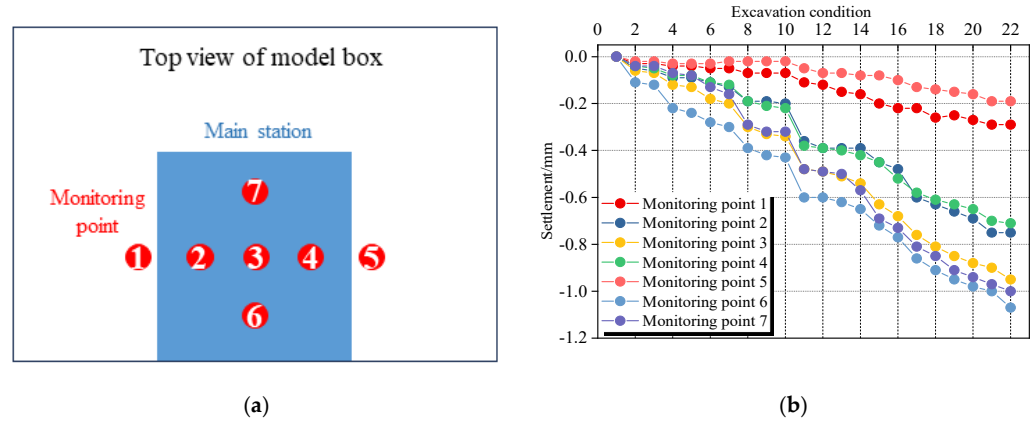


Figure 6. Ground settlement monitoring arrangement and monitoring results. (a): Settlement monitoring point layout. The blue block in the figure (a) is the main station. The red points is the arrangement of the eight monitoring points. (b): Patterns of change at different settlement monitoring sites.

3.3. Changing Law of Internal Force of Support Structure

The stress of the supporting pile is measured by the earth pressure box buried at the top of the pile. The stress release of the surrounding rock can be measured before the installation of the middle column, and the stress variation trend can be measured after the installation of the middle column. Figure 7 illustrates the trend of the overburden stress on the gypsum arch. It is evident that the overburden depths in the central column force correspond to 6.3 m, 12.6 m, and 18.9 m, respectively, according to the similarity ratio relationship. During the construction of the arch cover, the existence of the gypsum arch cover results in a small stress release of the overburden on the arch. The peak of stress reduction occurs at the position where the thickness of the overburden is 36 cm, with a stress value of 1.2 kPa. This corresponds to the working condition of the demolition of the central diaphragm wall. Prior to the removal of the diaphragm wall, there is a slow release of overburden pressure, but not much reduction. Following the removal of the diaphragm wall, the soil above compressed downwards but remained confined by the arch cover support structure. This led to an increase in internal pressure, which eventually stabilized. The fluctuations in soil pressure within the overburden were insignificant, and the overall condition has remained stable.

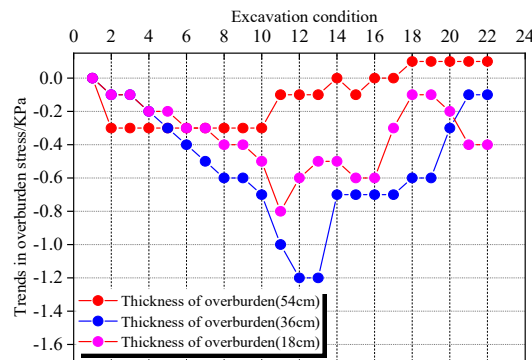


Figure 7. Trend of overburden stress on gypsum arch.

Figure 8 illustrates the force changes above the gypsum arch cap after excavation. Negative values indicate downward compression of the arch, resulting in compressive stresses, while positive values indicate upward bulging of the arch cap, resulting in tensile stresses. Tensile stresses were observed at the location of the right arch gridle during the construction of the arch cap while excavating side drift A. The excavation of the left drift altered the state of the perimeter rock of the arch, resulting in slight uneven stress at the

left and right ends of the arch cap. However, the excavation of side drift B caused the surrounding rock below the left arch haunch to hollow out, and the surrounding rock above squeezed the arch cover, returning the left arch crown to a state of compressive stress.

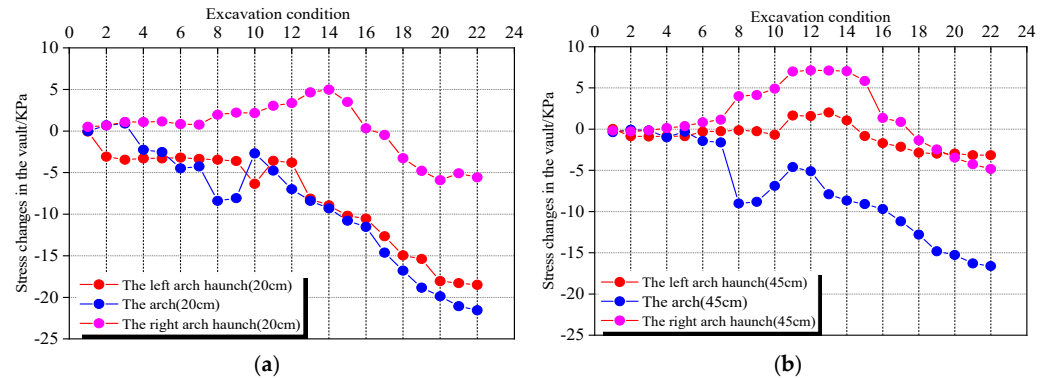


Figure 8. Variation curve of internal force of the arch. (a): Stress trends in the arch and arch haunch at 20 cm. (b): Stress trends in the arch and arch haunch at 45 cm.

The maximum compressive stress in the arch is located at the top, with a maximum value of 21.5 kPa. The deformation stress at 20 cm of the monitored section is greater than that at 45 cm. The addition of the central column resulted in a reduction of compressive stress in the arch cap. Analysis showed that solidification of the gypsum at the top of the pile caused expansion, which in turn lifted the arch cap, counteracting some of the extruded stresses from the downward deformation of the arch cap. During the removal of the initial support of the central drift, the arch cover experienced rapid stress release. Subsequently, after the removal of the initial support of the central drift, the stress release rate of the arch cover gradually slowed down and eventually stabilized.

Figure 9 illustrates the stress trends in the arch feet under various operating conditions. As shown in the figure, the stresses in the left and right arch feet exhibit only minor fluctuations during the mid-guideway stage of the excavation. The excavation of the side drifts led to the release of compressive stresses at the foot of the arch, resulting in a significant reduction in compressive stresses on the same side. During excavation of the lower surrounding rock, the arch foot bears part of the upper earth pressure transmitted by the arch cover, leading to increased compressive stress. To prevent local stress concentration in the arch foot, partial reinforcement of the left and right arch foot areas should be considered. This will help the arch foot withstand the pressure from above and avoid being crushed.

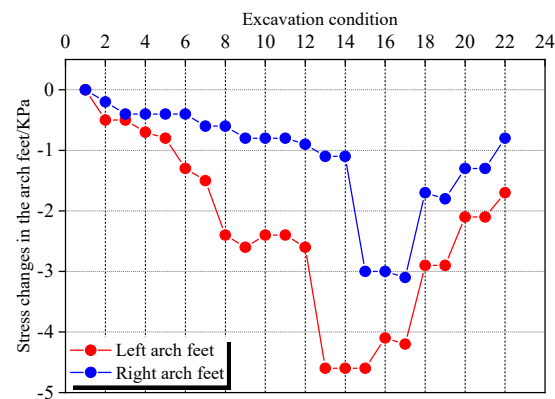


Figure 9. Variation stress of arch feet.

3.4. Analysis of the Support Effect of the Central Column

Due to the inability to conduct an on-site analysis of the support effect of neutral columns on the arch cover in practical engineering scenarios, the study subsequently investigated the support effect of neutral columns on the arch cover during the construction process using arch construction methods. Following the completion of the experiments, the neutral columns were dismantled, and data on the deformation of the arch cover and ground settlement before and after dismantling were recorded. This enabled an exploration of the support effect of neutral columns on the arch cover. The changes in arch displacement and ground settlement after the removal of the central column are shown in Tables 7 and 8 (Figure 10). The table shows that the deformation of the arch and ground settlement increased significantly after the demolition of the central column. The maximum year-on-year increase in the arch settlement was 79.41%, and the maximum year-on-year increase in the ground settlement was 97.20%. The closer to the central position of the arch cap, the more pronounced the increase in settlement. The presence of the central column is crucial for supporting the arch cover and controlling the deformation and settlement of the rock and soil above it.

Table 7. Changes in arch displacement before and after central column removal.

Monitoring Point	Left Arch Haunch 20 cm/mm	Arch Crown 20 cm/mm	Right Arch Haunch 20 cm/mm	Left Arch Haunch 45 cm/mm	Arch Crown 45 cm/mm	Right Arch Haunch 45 cm/mm
Before the removal of the central column	0.28	0.34	0.2	0.18	0.22	0.17
After the removal of the central column	0.41	0.61	0.31	0.29	0.39	0.29
Percentage increase	46.43%	79.41%	55.00%	61.11%	77.27%	70.59%

Table 8. Changes in ground settlement before and after central column removal.

Monitoring Point	Point 1 /mm	Point 2 /mm	Point 3 /mm	Point 4 /mm	Point 5 /mm	Point 6 /mm	Point 7 /mm
Before the removal of the central column	−0.29	−0.78	−0.96	−0.74	−0.19	−1.07	−1.05
After the removal of the central column	−0.45	−1.42	−1.81	−1.37	−0.3	−2.11	−1.92
Percentage increase	55.17%	82.05%	88.54%	85.14%	57.89%	97.20%	82.86%



Figure 10. Comparison results before and after removal of the central column. (a): Before the removal of the central column. (b): After the removal of the central column.

4. Conclusions

Based on the underground concealed excavation station project of Tianhe Road Station of Guangzhou Metro Line 10 in China, this paper designed and established a model test device for the arch cover method by using the existing model box in the laboratory, and carried out an indoor model box test study of the arch cover method for underground stations, and analyzed the influence of different excavation conditions on the stress patterns of the arch cover, ground settlement, arch haunch, arch foot, and central column. The main conclusions of the paper are as follows:

(1) Better overtopping reduces the settlement of the arch, with the maximum settlement of the arch located near the top of the arch. The removal of the diaphragm wall primaries has a greater effect on the settlement of the arch compared to the other conditions. Among them, the removal of the initial support of the diaphragm wall is the single condition that leads to the largest settlement increment in the middle of the arch. The effect of the excavation of the middle guideway stage on the settlement of the arch haunch is not obvious, and the excavation of the lower body will still disturb the rock layer above, resulting in a larger amount of settlement.

(2) The ground settlement generally occurs at the same location as the arch settlement, but in practice, the arch settlement will occur earlier than the ground settlement. If there are sandy strata above the tunnel, the ground settlement may be greater than the arch settlement due to the liquefaction of the strata caused by excavation vibration.

(3) The influence of arch cover excavation on overburden pressure is small, and the supporting structure is more conducive to controlling the deformation of overburden. The central column bears most of the compressive stress over the arch cap, showing a trend of first decreasing and then increasing. The central column gradually bears the pressure above the arch since the removal of the diaphragm wall and increases to the maximum value after the excavation is completed. The upper region of the arch cover is mainly subjected to extrusion stress, and the maximum extrusion stress of the arch cover occurs near the middle of the arch cover. The left and right arch feet did not change significantly during the excavation of the central drift, and the stress in the arch feet decreased greatly during the excavation of the side drift. After excavating the lower rock body, the left and right arch feet began to bear the pressure of the soil body above, resulting in an increase in the arch foot stress.

(4) The presence of the central column has a greater impact on the settlement of the arch and the ground settlement, and the closer to the middle of the arch the more pronounced the magnitude of deformation is after the removal of the central column.

Author Contributions: Conceptualization, W.Y.; Methodology, W.Y. and T.L.; Validation, W.P.; Formal analysis, W.Y. and M.X.; Investigation, M.X. and T.L.; Data curation, M.X. and W.P.; Writing—original draft, W.Y. and W.P.; Writing—review & editing, T.L.; Supervision, T.L. All authors have read and agreed to the published version of the manuscript.

Funding: This research was funded by the National Natural Science Foundation of China grant number [No. 52374108].

Institutional Review Board Statement: Not applicable.

Informed Consent Statement: Not applicable.

Data Availability Statement: The data presented in this study are available on request from the corresponding author. The data are not publicly available due to the subsequent paper writing also needs to use the paper data.

Conflicts of Interest: Authors Wangxing Yang, Mingkai Xu, Wenxiang Peng and Taoying Liu was employed by the company China Railway 16th Bureau Group Corporation. The remaining authors declare that the research was conducted in the absence of any commercial or financial relationships that could be construed as a potential conflict of interest.

References

1. Wei, L.; Chuan, H. Survey on construction methods for metro stations. *West-China Explor. Eng.* **2004**, *7*, 109–112. (In Chinese)
2. Guo, Z. A New underground excavation construction method for subway stations-arch cover Method. *Urban Rail Transit Res.* **2012**, *15*, 145–148. (In Chinese)
3. Zhang, G.; Du, Z.J.; Song, J.Q.; Cai, J.D.; Tao, T.J. Monitoring and analysis of excavation-induced subsidence of subway station constructed by arch cover method and control measures. *Chin. J. Rock Mech. Eng.* **2012**, *31* (Suppl. S1), 3413–3420. (In Chinese)
4. Wang, D. Study on Evaluation System of the Impact of Metro Station Construction with Arch Cover Method on the Surrounding Environment. Master's Thesis, Shijiazhuang Railway University, Shijiazhuang, China, 2022. (In Chinese).
5. Yu, L.; Zhang, D.; Fang, Q.; Cao, L.; Xu, T.; Li, Q. Surface Settlement of Subway Station Construction Using Pile-Beam-Arch Approach. *Tunneling Undergr. Space Technol.* **2019**, *90*, 340–356. [[CrossRef](#)]
6. Fang, Q.; Zhang, D.; Wong, L.N.Y. Shallow Tunnelling Method (Stm) for Subway Station Construction in Soft Ground. *Tunn. Undergr. Space Technol.* **2012**, *29*, 10–30. [[CrossRef](#)]
7. Liu, B.; Li, H.; Li, L.; Zhao, Q.; Gao, J. Construction Technique of Vertical Shafts Excavation Above Subway Tunnel. *Geotech. Geol. Eng.* **2021**, *39*, 4225–4235. [[CrossRef](#)]
8. Shang, Y.; Du, S.; Han, T.; Shao, B. Case Study on Deformation Control of Upper-Soft and Lower-Hard Large Span Tunnel Station Using Combined Control Technology and Monitoring Demonstration. *Sains Malays.* **2017**, *46*, 2091–2099. [[CrossRef](#)]
9. Wang, J.; Huo, Q.; Song, Z.; Zhang, Y. Study on Adaptability of Primary Support Arch Cover Method for Large-Span Embedded Tunnels in the Upper-Soft Lower-Hard Stratum. *Adv. Mech. Eng.* **2019**, *11*, 1687814018825375. [[CrossRef](#)]
10. Song, Z.; Cao, Z.; Wang, J.; Wei, S.; Hu, S.; Niu, Z. Optimal Analysis of Tunnel Construction Methods through Cross Passage from Subway Shaft. *Adv. Civ. Eng.* **2018**, *2018*, 5181954. [[CrossRef](#)]
11. Ritter, S.; DeJong, M.J.; Giardina, G.; Mair, R.J. Centrifuge Modelling of Building Response to Tunnel Excavation. *Int. J. Phys. Model. Geotech.* **2018**, *18*, 146–161. [[CrossRef](#)]
12. Dong-Hyun, S.; Seung-Ho, L. The Case of Measurement for Shallow Soil Tunnel with Pre-Supported Nail Method. *J. Korean Geo-Environ. Soc.* **2012**, *13*, 69–79.
13. Oreste, P.P.; Dias, D. Stabilisation of the Excavation Face in Shallow Tunnels Using Fibreglass Dowels. *Rock Mech. Rock Eng.* **2012**, *45*, 499–517. [[CrossRef](#)]
14. Cao, L.; Fang, Q.; Zhang, D.; Chen, T. Subway Station Construction Using Combined Shield and Shallow Tunnelling Method: Case Study of Gaojiayuan Station in Beijing. *Tunn. Undergr. Space Technol.* **2018**, *82*, 627–635. [[CrossRef](#)]
15. Shen, G.; Zhang, D.; Chen, T. Ground Surface Settlement Analysis of Metro Tunnel Using Pba Method: A Case Study of the Su-Huang Interval. *Electron. J. Geotech. Eng.* **2016**, *21*, 10055–10068.
16. Liu, J.; Wang, F.; He, S.; Wang, E.; Zhou, H. Enlarging a Large-Diameter Shield Tunnel Using the Pile-Beam-Arch Method to Create a Metro Station. *Tunn. Undergr. Space Technol.* **2015**, *49*, 130–143. [[CrossRef](#)]
17. Xu, X.; Li, Z.; Fang, Q.; Zheng, H. Challenges and Countermeasures for Using Pile-Beam-Arch Approach to Enlarge Large-Diameter Shield Tunnel to Subway Station. *Tunneling Undergr. Space Technol.* **2020**, *98*, 103326. [[CrossRef](#)]
18. Tian, X.; Song, Z.; Zhang, Y. Monitoring and Reinforcement of Landslide Induced by Tunnel Excavation: A Case Study from Xiamaixi Tunnel. *Tunn. Undergr. Space Technol.* **2021**, *110*, 103796. [[CrossRef](#)]
19. Liu, X.; Liu, Y.; Qu, W.; Tu, Y. Internal Force Calculation and Supporting Parameters Sensitivity Analysis of Side Piles in the Subway Station Excavated by Pile-Beam-Arch Method. *Tunneling Undergr. Space Technol.* **2016**, *56*, 186–201. [[CrossRef](#)]
20. Wang, F.W. Model Experimental Study on Mechanical Behaviour of Large-Span Underground Station Construction. Master's Thesis, Shijiazhuang Railway University, Shijiazhuang, China, 2014. (In Chinese).
21. Liu, G. Research on Construction Mechanical Behaviour of Puhuangyu Underground Station. Master's Thesis, Southwest Jiaotong University, Chengdu, China, 2014. (In Chinese).
22. Lei, M.; Peng, L.; Shi, C.; Wang, L.; Li, Z. Model Research on Failure Mechanism and Lining Stress Characteristics of Shallow Buried Tunnel Under Unsymmetrical Pressure. *J. Cent. South Univ.* **2013**, *44*, 3316–3325.
23. Xiao, J. Stability Analysis of Peripheral Rock and Supporting Structure of Shallow Buried Biased Tunnel in Soil-Stone Junction Stratum. Master's Thesis, Chang'an University, Xi'an, China, 2020. (In Chinese).
24. Li, W.; He, C.; Chen, X. Model test study on the construction of metro station with three consecutive arches by shield method. *Eng. Mech.* **2010**, *27*, 245–248. (In Chinese)
25. Huang, K.; Qing, S.; Xie, G.; Chen, K.; Zeng, S.; Huang, B. Simulation experiment of similar materials of cement and gypsum. *West. China-Explor. Eng.* **2003**, *12*, 127–129. (In Chinese)
26. Dong, C.; Yang, J.; Hu, T. Research on Analogous Material Model Test for Highway Tunnels. *Mod. Tunn. Technol.* **2010**, *47*, 11–16. (In Chinese)

Disclaimer/Publisher's Note: The statements, opinions and data contained in all publications are solely those of the individual author(s) and contributor(s) and not of MDPI and/or the editor(s). MDPI and/or the editor(s) disclaim responsibility for any injury to people or property resulting from any ideas, methods, instructions or products referred to in the content.